TEM Analysis of Nanosize Pb Inclusions in Al

U. Dahmen[1], E. Johnson[1,2], SQ. Xiao[3] and A. Johansen[2]

[1]*National Center for Electron Microscopy, LBNL, Berkeley, CA 94720, USA*
[2]*Department of Physics, Niels Bohr Institute, Univ. of Copenhagen, Denmark*
[3]*Riga Analytical Lab, Inc., 3375, Scott Blvd, Suite 132, Santa Clara, CA 95054, USA*

(Received: Jan. 31, 1997 Accepted: Mar. 10, 1997)

Abstract

This work presents results from an ongoing investigation of nanoscale Pb inclusions in Al, ranging from about two to a few tens of nanometers in size. The equilibrium shapes of inclusions in the bulk, at twin boundaries and at grain boundaries are characterized by high resolution electron microscopy. Bulk inclusions are found to approximate a cuboctahedral shape which tends to become asymmetric at smaller sizes. The finding that inclusion dimensions in bulk Al tend to follow preferred "magic sizes" follows from a balance of strain and interfacial energies. Inclusions at twin boundaries form strongly faceted twinned bicrystals whereas inclusions at grain boundaries form single crystals faceted toward one grain and rounded toward the other. These results can be understood in terms of a modified Wulff construction first proposed by Winterbottom.

1. Introduction

The optimum shape of a crystal in equilibrium with its vapor is the shape which minimizes its surface energy for a given volume. If the surface energy σ as a function of orientation is known, the equilibrium shape for a particle of fixed size can be determined using the Wulff construction [1]. Experiments on micrometer-size spheres equilibrated in a closed system have shown that near their melting point, most face centered cubic metals, e.g. Pb, exhibit equilibrium shapes that are spheres truncated by flat {111} facets with a maximum interface energy anisotropy of typically a few percent [2,3].

By comparison, a precipitate or inclusion in a solid matrix is subject to more complex constraints. The equilibrium shape of a solid inclusion minimizes the sum of its interface energy and its elastic energy. In addition, the crystallographic constraints are more stringent because the equilibrium shape must include the symmetry of the bicrystal, and thus depends on the orientation relationship between the lattices. Although a large body of work on shapes of precipitates in age hardening alloy systems exists [e.g.4,5,6], most of these are established under non-equilibrium conditions, and inclusion shapes usually continue to evolve with continued heat treatment [7]. It is therefore difficult to explore the effects of crystallography and of interfacial and elastic energy on the equilibrium shapes of precipitates in age-hardening systems. The Al-Pb system overcomes most of these difficulties. Both components are face-centered cubic, leading to a particularly simple crystallography. Pb and Al have negligibie mutual solid solubility and do not react, leading to especially simple thermodynamic conditions. Pb has a low melting point, and shape equilibrium can readily be obtained by melting and resolidifying the inclusions. For these reasons, Al-Pb is a good model alloy, and a significant amount of work has already been reported on Pb inclusions in bulk Al, most of it focused on the unusual melting and solidification behavior [8-15].

In this work, we describe some results from an ongoing investigation of Pb inclusions in Al [16-20], concentrating on the effect of internal interfaces on equilibrium shapes. After a brief review of recent results on the shape of small Pb precipitates in bulk Al, we illustrate and analyze the effect of twin boundaries and grain boundaries on their equilibrium shape. Using a modification of the Wulff construction due to Winterbottom [21], and to Lee and Aaronson [22], we show how it is possible to understand the complex composite shapes of inclusions at internal interfaces.

2. Experimental Procedure

Nanosized Pb inclusions were produced by ion implantation of Pb into 1000Å thick Al films. The films were grown by vapor deposition on single crystal Si substrates at 280°C and subsequently implanted from the Al surface with 60keV Pb ions to an average concentration of about 1% at temperatures between 150 and

250°C. The films were back-thinned from the Si side to electron-transparency and examined by high resolution electron microscopy (Berkeley Atomic Resolution Microscope, operating at 800kV). To determine the optimum visibility conditions as a function of defocus, foil thickness, inclusion size and position within the foil, extensive image simulations were carried out [17]. Under optimum conditions, the particle dimensions could be measured with an accuracy of ± one lattice spacing.

3. Results

Al-Pb forms a simple monotectic alloy system with negligible mutual solubility in the solid state. Both, the Al matrix and the Pb precipitates are face centered cubic, with lattice parameters of 4.05 and 4.95Å, respectively. Despite this large difference in lattice parameter, the precipitates generally adopted a parallel-cube orientation relationship with the matrix and were found to be free of defects [16].

3.1 Inclusions in The Bulk

The equilibrium shape of Pb inclusions in bulk Al equilibrated by melting and re-solidification was established by electron microscopy observations in <110> zone axis orientation. From images such as that in Figure 1 it could be deduced that their shape was that of a cuboctahedron, i.e. a regular octahedron bounded by eight {111} faces and truncated on the six{100} faces. In a <110> projection, four of the eight {111} facets and two of the six {100} facets are seen edge-on. Following Herring [23] the ratio of interfacial energies can be measured directly from the equilibrium shape as the ratio of distances between pairs of interface facets. Measurements on melt spun alloys containing larger particles, a few hundred nanometers in size, have shown a ratio of interface energies $\sigma_{100}/\sigma_{111} = 1.15$ [10].

Figure 1 shows a high resolution image of a smaller inclusion, produced by ion implantation. The crystal lattice is viewed along a <110> direction where the separation between close-packed atomic planes is 0.23nm for the Al matrix and 0.29nm for the Pb inclusions. Because the inclusions are fully embedded within the Al matrix, the overlap of the two lattices gives rise to a moiré contrast effect. The inclusion is seen to be symmetrical in shape with a separation of 5.1nm between both pairs of {111} facets and 6.0nm between {100} facets. The aspect ratio of 1.18 for this inclusion is slightly larger than that of larger particles. By comparison, the inclusion shown in Figure 2 is only 2.6nm in size and shows no {100} facets at all, corresponding to an aspect ratio of $\sqrt{3}$. A large variation in the {100}/{111} anisotropy between different particles was typical for small inclusions. Measurements on a significant number of inclusions in the size range between 2 and 10nm showed a mean aspect ratio of 1.28±0.12 [24,16], significantly higher than that of 1.15

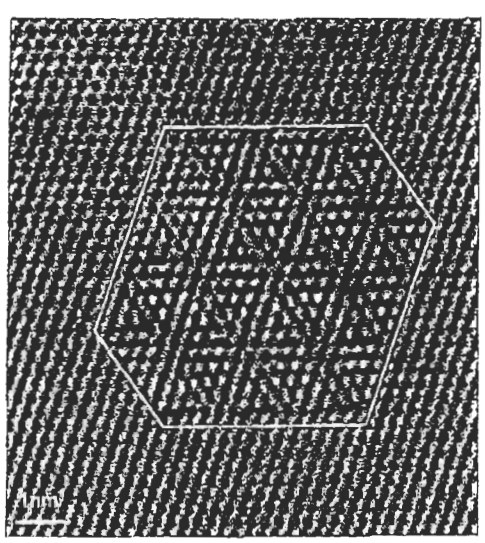

Fig. 1 High resolution micrograph of nanoscale Pb inclusion embedded in an Al matrix. Moiré fringes arise from interference between overlapping Pb and Al lattices. This inclusion is symmetrical in shape and displays an anisotropy of $\sigma_{100}/\sigma_{111} = 1.18$.

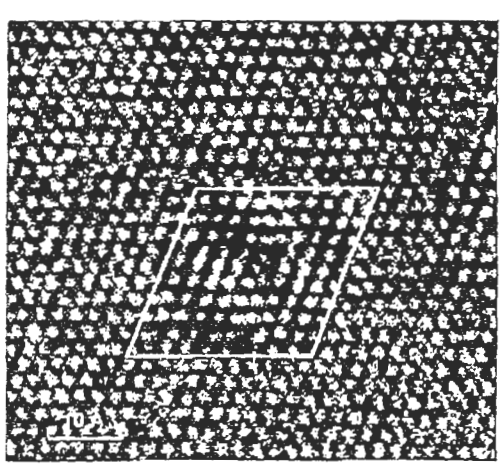

Fig. 2 Small octahedral inclusion only 2.6nm in size. The inclusion is symmetrical in shape but has no {100} truncations, leading to an apparent anisotropy of >1.73.

established for larger inclusions [10].
In addition, it was found that most particles were less symmetrical than those shown above. Typical inclusions in this small size regime varied in size and shape, occasionally showing asymmetrical truncations on {100} planes and often with different extent of the {111} facets. The same asymmetrical shape was often observed to be re-established after in-situ melting and re-solidification. Unlike the larger cuboctahedral particles, the equilibrium shape of these small inclusions thus includes irregular polyhedra, mainly bounded by eight {111} and to a lesser extent by some (though often not all six) {100} facets. To characterize the inclusion size accurately, the dimensions in different directions were measured separately as the separation between opposite {111} facets. A histogram of these measurements (Figure 3) showed the surprising result that the inclusions appeared to prefer certain "magic" sizes while avoiding others [18].
It has recently been shown that these observations can be understood as a consequence of the confinement within a solid [18]. Although most of the large volume difference between Pb and Al is accommodated by lattice vacancies, this accommodation can occur only to the nearest discrete lattice distance. There thus remains a *residual* elastic distortion whose energy oscillates with an amplitude that is directly proportional to inclusion size (see dashed line in Figure 3) whereas the interface energy is proportional to the square of the size. The residual elastic strain energy therefore dominates in the small size regime investigated here, while the interface energy becomes the dominant term at larger sizes. It can be concluded that Pb inclusions in bulk Al adopt size dependent equilibrium shapes with preferred dimensions that follow a sequence of "magic sizes" similar to those observed for free clusters. Whereas in free clusters, magic sizes occur when coordination shells are filled, for inclusions, magic sizes are found whenever the two lattices are commensurate.

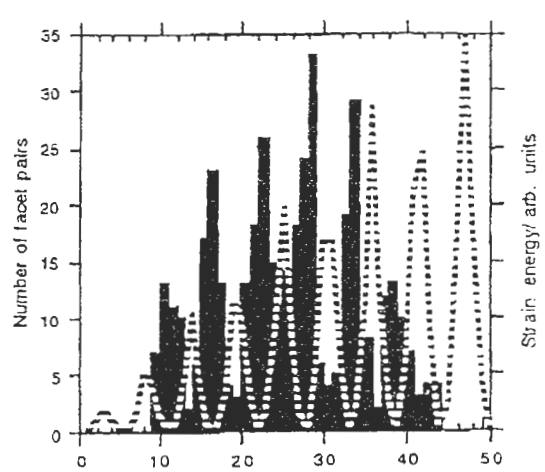

Fig. 3 Histogram of size distribution showing periodic gaps at certain sizes, anti-correlated with the residual strain energy (dashed line) [18].

3.2 Inclusions at twin boundaries

At internal interfaces such as twin and grain boundaries, Pb nucleates preferentially to form inclusions with more complex shapes [19,20]. Figure 4 shows a typical Pb inclusion at a twin boundary. It is apparent that the inclusion is twinned as well, thus forming a compound shape made of two partial octahedra joined along a common {111} face.
As illustrated in Figure 5, the equilibrium shape of such an inclusion can be determined using a variation on the Wulff construction, first

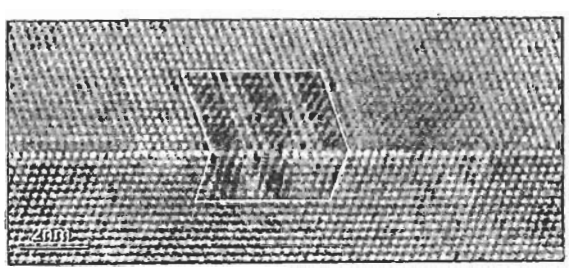

Fig. 4 Pb inclusion at twin boundary in Al exhibiting composite shape of two twin-related inclusions joined along the twin boundary. Note that the inclusion is not centered on the boundary and contains a reentrant facet junction.

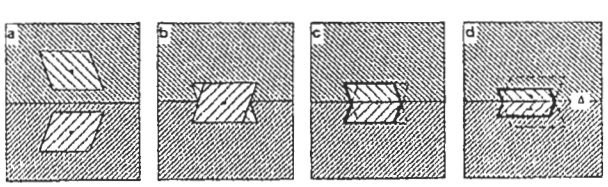

Fig. 5 Schematic illustration of Winterbottom construction for the equilibrium shape of an inclusion on a twin boundary. The two equilibrium shapes in each grain shown in (a) are superimposed with their Wulff points on the boundary (b) resulting in a compound shape when each is truncated by the twin boundary (c). The elongated equilibrium shape in (d) results when the twin boundary energy in Al is higher by an amount Δ than the twin boundary energy in Pb and the two Wulff points are displaced by $\Delta=\sigma_{twinAl}-\sigma_{twinPb}$.

proposed by Winterbottom for crystals on surfaces [21], and subsequently modified by Lee and Aaronson [22] for precipitates at grain boundaries. Imagine two equilibrium-shaped inclusions in a crystal containing a twin boundary (a). Superimpose the two equilibrium shapes with their Wulff points on the twin boundary (b) and discard from each inclusion the part that overlaps the opposite grain (c). The resulting inclusion is twinned and has the same aspect ratio of height to width as each of the untwinned inclusions in the bulk crystals. This is the equilibrium shape if the difference Δ in the twin boundary energies in the matrix and the inclusion is zero.

If the twin boundary energy in the inclusion is higher than that in the matrix, the equilibrium shape will be taller and narrower whereas in the opposite case, if the twin boundary energy is smaller in the inclusion, the shape will be broader, covering more of the twin boundary. This latter case is shown in (d) and corresponds to partial wetting of the twin boundary by the inclusion. Note that for simplicity Figure 5 has been drawn for a perfect octahedral shape, ignoring any truncations on the {100} faces. Although this is in agreement with Figure 4, many other observations show that {100} truncations can in fact be part of the inclusion shapes on twin boundaries, and a more accurate analysis will have to take this into account. However, at present the variability of observed shapes and aspect ratios of twin boundary inclusions is too large to warrant a more accurate analysis. Given the size dependence and preference for dimensions of magic sizes of bulk inclusions in the same size range, a quantitative analysis is likely to require larger inclusions.

However, it is worthwhile to point out some interesting features of the equilibrium shape of such twin boundary inclusions. As seen from Figures 4 and 5, for this type of inclusion, the equilibrium shape is no longer confined to a convex shape. Both protruding and reentrant angles can be present in the equilibrium shape. It is also apparent that the twin boundary does not have to pass through the center of the inclusion. Asymmetrical shapes, with the twin boundary passing through some part of the inclusion will have the same balance of interfacial energies and hence be favorable. Many inclusions were indeed observed to be asymmetrical.

3.3 Inclusions at Grain Boundaries

When Pb nucleates at grain boundaries, it forms compound shapes that are more complex than those on twin boundaries [19]. Grain boundary inclusions ("allotriomorphs" [22]) tend to be sharply faceted toward one grain and rounded toward the other grain.

A typical inclusion at a 90° <110> tilt grain boundary is shown in Figure 6. Its size is significantly larger than that of inclusions in the bulk or at twin boundaries. The boundary is a 90° <110> tilt boundary in symmetrical orientation. The relative orientation of the two grains is indicated schematically with rectangles which are parallel to the projected unit cells of the Al lattices. Although it appears that the inclusion is made of two distinct parts joined along the interface, this inclusion is actually a single crystal. The different moiré patterns in the two grains result

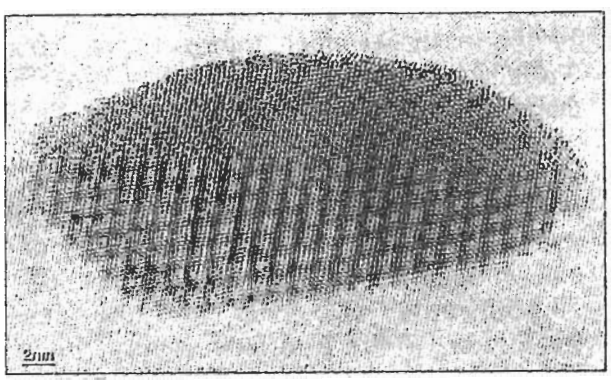

Fig. 6 Large Pb inclusion on a high angle grain boundary in Al showing typical composite shape with one rounded and one faceted segment. The inclusion is a single crystal but forms different moiré patterns with the two grains.

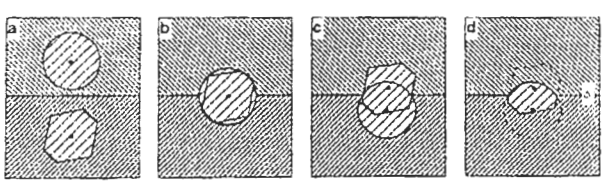

Fig. 7 Schematic illustration of the modified Wulff construction for a grain boundary inclusion [19]. Two different Wulff shapes for two different orientation relationships with the matrix crystal are outlined in (a). The lattice orientation is indicated by the direction of cross hatching. The two shapes are superimposed with their Wulff points on the boundary in (b) and displaced by an amount Δ in (c). The equilibrium shape is the intersection of the two individual Wulff shapes (d). Note that by comparison with Figure 5, the boundary does not cross the inclusion.

from interference between a single crystal of Pb with a bicrystal of Al. Thus, in the lower, faceted part of the inclusion the Pb lattice is in parallel orientation with the Al lattice, while the upper, rounded part is the same Pb crystal rotated by 90° with respect to the Al lattice. As a result, the interface structures are very different, leading to correspondingly different interfacial energies and anisotropies.

Because this inclusion is a single crystal its equilibrium shape is determined by a slightly different procedure than that used for twin boundary precipitates above. In the case of twin boundary precipitates, both segments of the particle were in parallel orientation with their respective grain, leading to a particle that was itself twinned. In the case of grain boundary precipitates, the two segments have a different orientation relationship with their respective grains, but the particle is a single crystal.

To use the modified Winterbottom construction for this case, we must intersect two different Wulff shapes across the boundary. The Wulff shape for the lower crystal is the familiar cuboctahedron while that for the upper crystal (the Wulff shape of a Pb crystal rotated 90° with respect to its embedding Al matrix) is approximated as a sphere. The radius of the sphere relative to the dimensions of the cuboctahedron is given by the relative magnitude of the interface energy. Figure 7 illustrates schematically a similar sequence of operations as that in Figure 5. In (a) the equilibrium Wulff shapes of a Pb inclusion in each crystal are shown, with the hatching indicating the lattice orientation. In (b), these two shapes are superimposed on the boundary and then moved past each other until their Wulff points are a distance Δ apart, where Δ is the energy of the grain boundary. The equilibrium shape is again the composite shape made from the segments of the individual Wulff shapes that remain in their original matrix grain (d). Note that when the two segments are joined, they form a single crystal, thus eliminating a piece of the grain boundary.

The constructions shown in Figures 5 and 7 are illustrated in two dimensions. As pointed out before [22], the intersection of two different Wulff shapes across a planar interface is usually not a planar curve, but a curve in three-dimensional space. The analysis shown here is thus an oversimplification. In reality, either the intersecting shapes or the boundary will have to be distorted to become geometrically compatible. Note that this is not the case for a twinned inclusion on a twin boundary because the two intersecting shapes are mirror-related and thus intersect in a planar curve (on the mirror plane). In principle, this is possible for any symmetrical grain boundary, including that shown in Figs 6 and 7. However, the energy of a symmetrical bicrystalline inclusion which is being traversed by the grain boundary is apparently higher than that of an asymmetrical single crystalline inclusion in which the grain boundary follows one side of the interface.

Because of the mirror symmetry of a symmetrical grain boundary, there are two mirror-related and energetically equivalent orientations of the grain boundary inclusion (rounded side up or down). Both orientations were indeed observed, and in one case, at elevated temperature, such an inclusion was found to change from one orientation variant to the other over the period of a few seconds.

Unlike the inclusions at twin boundaries, those at general grain boundaries were found to depend strongly on the boundary inclination. While twin boundaries were only found in a single inclination (the {111} coherent twin plane), the grain boundaries in the mazed bicrystal structure investigated here take on all inclinations in the <110> zone. An extension of the modified Wulff construction describes the shapes observed at most of these interface inclinations well. However, a full discussion of these observations is outside the scope of this manuscript.

4. Summary

The equilibrium shape of Pb inclusions in a solid Al matrix depends on size and location. Despite a large misfit between the two lattices, Pb inclusions tend to be accurately aligned with the Al matrix. Inclusions located in bulk Al are free of defects, sharply faceted on {111} and to a lesser extent on {100} planes and assume dimensions of "magic sizes". This behavior is due to the oscillatory nature of the residual strain energy which dominates in the small size regime. For larger sizes, the interface energy becomes more important, and larger inclusions take on a cuboctahedral shape.

Pb located at twin and grain boundaries, forms composite shapes made from segments of two Wulff shapes joined along the interface. At twin boundaries, Pb forms bicrystal inclusions of nearly symmetrical shape. By comparison, at grain boundaries, Pb forms single crystal

inclusions with asymmetrical shape. Both observations can be understood in terms of a modified Wulff construction.

Acknowledgment
This work is supported by the Director, Office of Energy Research, Office of Basic Energy Sciences, Materials Sciences Division of the U.S. Department of Energy under Contract No. DE-AC03-76SF000098, and the Danish National Sciences Research Council.

Referenced

1. G. Wulff, Z. Krystall. Mineral. 34, 449, 1901
2. J.C. Heyraud and J.J. Métois, J. Cryst. Growth 50, 571 (1980)
3. J.C. Heyraud and J.J. Métois, Surf. Sci. 128, 334 (1983)
4. D.A. Porter, K.E. Easterling, "Phase Transformations in Metals and Alloys", Van Nostrand Reinhold, New York 1981
5. J.W. Martin, "Micromechanisms in particle-hardened alloys", Cambridge University Press, Cambridge 1980
6. K.B. Alexander, F.K. LeGoues, H.I. Aaronson and D.E. Laughlin, Acta Met. 32, 2241 (1984)
7. R.M. Aikin Jr, M.R. Plichta, Acta Met. 38, 77 (1990)
8. M. Roth, G.C. Weatherly and W.A. Miller, Can. Met. Quarterly, 14, 287 (1975)
9. K.L. Moore, K. Chattopadhyay and B. Cantor, Proc. Roy. Soc. Lond. A414, 499 (1987)
10. D.L. Zhang and B. Cantor, Scr. Met. 24, 751 (1990)
11. K.L. Moore, D.L. Zhang and B. Cantor, Acta Met. Mat. 38, 1327 (1990)
12. E. Johnson, L. Gråbæk, J. Bohr, A. Johansen, L. Sarholt-Kristensen and H.H. Andersen, MRS Proc. 157, 247 (1990)
13. K.K. Bourdelle, A. Johansen, B. Schmidt, H.H. Andersen, E. Johnson, L. Sarholt-Kristensen, S. Steenstrup and L. Yu, Nucl. Instrum. Methods B80/81, 317 (1993)
14. L. Gråbæk, J. Bohr, H.H. Andersen, A. Johansen, E. Johnson, L. Sarholt-Kristensen, and I.K. Robinson, Phys. Rev. B 45, 2628 (1992)
15. L. Gråbæk, J. Bohr, E. Johnson, A. Johansen, L. Sarholt-Kristensen and H.H. Andersen Phys. Rev. Lett. 64, 934 (1990)
16. S. Q. Xiao, E. Johnson, S. Hinderberger, K. K. Bourdelle and U. Dahmen, J. Microscopy, 180, 61 (1995)
17. S.Q. Xiao, S. Paciornik,, R. Kilaas, E. Johnson and U. Dahmen, Proc. MSA 53, 646 (1995)
18. U. Dahmen, S.Q. Xiao, S. Paciornik, E. Johnson and A. Johansen, Phys. Rev. Lett., in press
19. Johnson, S. Hinderberger, S.Q. Xiao, U. Dahmen and A. Johansen, Interface Science, 3, 279 (1996)
20. E. Johnson, U. Dahmen, S.Q. Xiao and A. Johansen, Proc. MSA 54, 364 (1996)
21. W.L. Winterbottom, Acta Met. 15, 303 (1967)
22. J.K. Lee and H.I. Aaronson, Acta Met. 23, 799 (1975), Acta Met. 23, 809 (1975)
23. C. Herring, Phys. Rev. 82, 87 (1951)
24. B. Schmidt, MSc thesis, University of Copenhagen, (1992)19